Photochemical & Photobiological Sciences (2023) 22:745–759
https://doi.org/10.1007/s43630-022-00348-3

ORIGINAL PAPERS

The photophysics of 2-cyanoindole probed by femtosecond spectroscopy

Mahbobeh Morshedi[1] · Oliver Nolden[1] · Philipp Janke[1] · Wiebke Haselbach[1] · Michael Schmitt[1] · Peter Gilch[1]

Received: 16 September 2022 / Accepted: 24 November 2022 / Published online: 10 December 2022

Abstract

The photophysics of 2-cyanoindole (2-CI) in solution (water, 2,2,2-trifluoroethanol, acetonitrile, and tetrahydrofuran) was investigated by steady-state as well as time resolved fluorescence and absorption spectroscopy. The fluorescence quantum yield of 2-cyanoindole is strongly sensitive to the solvent. In water the quantum yield is as low as 4.4×10^{-4}. In tetrahydrofuran, it amounts to a yield of 0.057. For 2-CI dissolved in water, a bi-exponential fluorescence decay with time constants of ~1 ps and ~8 ps is observed. For short wavelength excitation (266 nm) the initial fluorescence anisotropy is close to zero. For excitation with 310 nm it amounts to 0.2. In water, femtosecond transient absorption reveals that the fluorescence decay is solely due to internal conversion to the ground state. In aprotic solvents, the fluorescence decay takes much longer (acetonitrile: ~900 ps, tetrahydrofuran: ~2.6 ns) and intersystem crossing contributes.

Graphical abstract

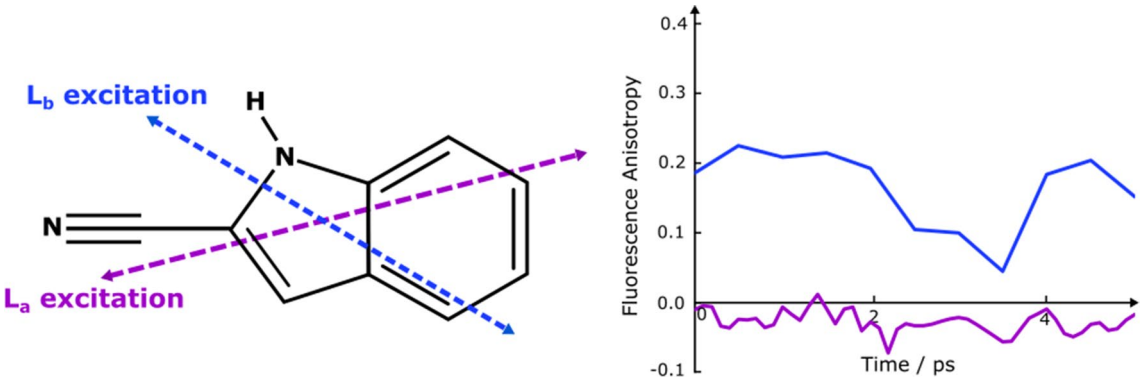

Keywords 2-Cyanoindole · Photophysics · Solvent effects · Time resolved spectroscopy · Fluorescence anisotropy · Triplet state

1 Introduction

The side chain of the amino acid tryptophan consists of the hetero-aromatic indole moiety. This moiety contributes strongly to the intrinsic fluorescence of proteins [1]. Substitution of the indole moiety may alter its fluorescence properties which can be exploited, for instance, in biophysical studies on proteins and peptides [2–6]. The cyano-substituent is hereby of particular interest. It exhibits strong negative inductive and mesomeric (resonance)

This publication is dedicated to Prof. Silvia E. Braslavsky, a pioneer in photobiology and photobiophysics, on the occasion of her 80th birthday.

✉ Peter Gilch
gilch@hhu.de

[1] Institut für Physikalische Chemie, Heinrich-Heine-Universität Düsseldorf, Universitätsstr. 1, 40225 Düsseldorf, Germany

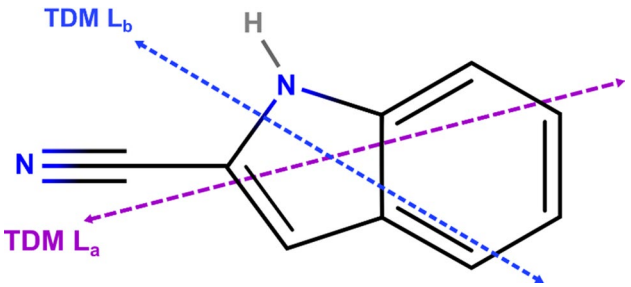

Scheme 1 Chemical structure of the molecule 2-CI. Purple and blue dashed arrows indicate the orientation of the transition dipole moments (TDM) of the L_a and L_b states [10]

effects on the chromophore [7]. It may, thus, substantially alter the electronic structure of indole. Due to its size, a cyano-substituent causes only a small steric effect [8]. Some cyanoindoles exhibit strongly solvent dependent fluorescence lifetimes and quantum yields [9]. For the title compound 2-cyanoindole (2-CI, structure in Scheme 1) dissolved in tetrahydrofuran (THF), a fluorescence lifetime of 2.9 ns was measured [9]. Dissolving the compound in dimethylsulfoxide (DMSO) reduces the lifetime to 0.4 ns. For water as a solvent, only an upper boundary of 0.05 ns for the lifetime was reported (see also ref. [10]). Due to this dependence, the fluorescence of 2-CI and other cyanoindoles can serve as a sensor of the local environment of an amino acid residue in a protein. The cyano-group further offers the possibility to probe this environment via vibrational spectroscopy [11–14].

Here, femtosecond fluorescence and UV/Vis absorption experiments on the photophysics of 2-CI are reported. The experiments aim at the fluorescence lifetime of 2-CI in water for which heretofore only an upper boundary has been reported (see above). Via time-dependent fluorescence anisotropy measurement, information on the emissive state (L_a or L_b) [15] is retrieved. With femtosecond UV/Vis absorption, transient states populated in the course of the fluorescence decay are detected. It is shown that in aprotic solvents intersystem crossing (ISC) contributes substantially to the decay. Experiments were conducted using solutions of 2-CI in water, 2,2,2-trifluoroethanol (TFE), acetonitrile (MeCN), and tetrahydrofuran (THF). TFE was selected to study the effect of the proticity on the photophysics. Like water, it is a protic solvent albeit with a lower dielectric constant. MeCN is a strongly polar but aprotic solvent and THF represents a solvent of moderate to small polarity.

2 Experimental section

2.1 Samples

2-CI (≥ 99.89%) was purchased from Chem Scene, thymidine (≥ 99.0%) from Sigma-Aldrich, water (HPLC gradient grade) from Fisher Chemical, 2,2,2-trifluoroethanol (99%) from Carbolution Chemicals, acetonitrile (≥ 99.9%) from Honeywell, tetrahydrofuran (≥ 99.9%) from Sigma-Aldrich. All chemicals were used as supplied. All measurements were performed at room temperature (~ 20 °C).

2.2 Steady-state measurements

Steady-state absorption spectra were measured with a Lambda 19 spectrometer from Perkin Elmer. Fluorescence spectra were recorded on a FluoroMax-4 (Horiba Scientific). The excitation wavelength was set to 260 nm. 1 cm fused silica cuvettes (Hellma Analytics) were employed for these measurements. To determine the fluorescence quantum yields Φ_{fl}, thymidine in water served as reference ($\Phi_{fl} = 1.32 \times 10^{-4}$ [16]). Fluorescence excitation spectra were obtained by detecting the fluorescence signal around 340 nm. For both, emission and excitation spectra, the optical densities were kept below 0.05 (per cm) to avoid inner filter effect. Spectra were corrected for the spectral sensitivity of the instrument.

2.3 Time resolved fluorescence measurements

A femtosecond fluorescence Kerr gating was used to trace the decay of 2-CI in water for 266 and 310 nm excitation pulses. A detailed description for this setup was given before [17, 18]. A Ti:Sa laser amplifier system (Libra, Coherent) served as pulse source with a repetition rate of 1 kHz, 100 fs pulse duration and a wavelength of 800 nm. To generate 266 nm pump pulses, a part of the output was first converted to a wavelength of 400 nm by frequency doubling (in a BBO crystal type I, 29°, 1 mm). Subsequently, from the doubled and the fundamental, the sum frequency was generated to yield a wavelength of 266 nm (in another BBO crystal, type II, 55.5°, 0.5 mm). The beam diameter was 80 µm (full width half maximum, FWHM) and the energy per pulse amounted to 1.1 µJ at the sample location. For the generation of 310 nm excitation pulses, a part of the output was fed in to a TOPAS-White non-collinear optical parametric amplifier system. The TOPAS was set to generate pulses peaking at 620 nm. By frequency doubling (BBO crystal, type I, 37°, 0.15 mm), they were converted to the pump wavelength of 310 nm with an energy per pulse of 0.9 µJ. The instrumental response function (IRF) was about 430 and 440 fs (FWHM) for 266 and 310 nm excitation light, respectively. The rather long IRF times can (partially) be attributed to the group velocity mismatch of fluorescence and gate light in the Kerr medium [19]. The optical gate operated as described before [18]. For the experiment with 266 nm excitation pulse, the integration time for each spectrum was set to 2.5 s. To record each scan, there were 50 steps from − 2 to 5 ps on a linear scale, then 35 steps on a logarithmic one up to 35 ps. For

this measurement, a total of 12 scans were averaged. For the measurement with 310 nm excitation pump, the integration time was set to 1 s. Each scan covered a time range of 40 ps which consisted of 80 equidistant steps. For this measurement, a total of 40 scans were averaged. The solutions were circulated by a peristaltic pump (REGLO Analog MS-2/8 from ISMATEC®) through a flow cell (custom made QX, Hellma Analytics) with 1 mm path length. Measurements on solutions of 2-CI (concentrations of ~ 24 µM and ~ 32 µM for the excitation of 266 and 310 nm light, respectively) as well as the neat solvent were performed. Solvent signals were subtracted from the solution ones after proper scaling.

2.4 Time resolved fluorescence anisotropy measurements

Measurements of the fluorescence anisotropy for both 266 and 310 nm excitation pulses were performed on the Kerr gate set up as well. To this end, a fluorescence signal $S_{||}(\lambda, t)$ with the pump pulse parallel to the first polarizer of the Kerr gate was recorded. Then the polarization of the pump light was rotated by 90° with a half-wave plate. Care was taken to ensure the same excitation energy for both polarizations were employed. The anisotropy was then calculated via [1]

$$r(\lambda, t) = \frac{S_{||}(\lambda, t) - S_{\perp}(\lambda, t)}{S_{||}(\lambda, t) + 2S_{\perp}(\lambda, t)}. \quad (1)$$

Thymidine in water was chosen for the calibrations of the set up. To record the parallel signal $S_{||}(\lambda, t)$ the solution was excited at 266 nm and the integration time amounted to 1 s. The time range covered was 7 ps. The range was divided in 70 equidistant steps. It was averaged over 13 delay line scans. The perpendicular signal $S_{\perp}(\lambda, t)$ was recorded with the same settings. Thymidine solution had a concentration of ~ 16 µM. The resulting anisotropy value from Eq. (1) was calculated. The initial anisotropy for thymidine in water was determined to be 0.31 ± 0.01. It compares favorably with the value of 0.35 reported by Gustavsson et al. [20]. For the anisotropy experiment on 2-CI solutions with 266 nm excitation, the same settings were applied to the parallel and perpendicular measurements. The integration time for each spectrum was set to 2.5 s. For recording each scan, there were 50 steps from − 2 to 5 ps linearly, then 35 steps on a logarithmic scale up to 35 ps. In total, 12 scans were averaged. To record the anisotropy measurement for the solution of 2-CI with 310 nm excitation light, the integration time amounted to 1 s. Each scan covered a time range of 40 ps which consisted of 80 linearly steps. For this measurement, a total of 7 scans were averaged. Time resolved anisotropy experiments were recorded as a function of detection wavelength and delay time, however, only one selected wavelength was shown (see result section). For dissolved 2-CI (concentrations of ~ 20 µM and ~ 30 µM for the excitation of 266 and 310 nm light, respectively) and the neat solvent data sets were recorded. After proper scaling the solvent signals were subtracted.

2.5 Femtosecond transient absorption

The experimental setup for femtosecond transient absorption measurements was described in depth elsewhere [21–23]. Briefly, for all measurements, a 1 kHz Ti:Sa femtosecond laser amplifier system (Libra, Coherent) was used to obtain the frequency-tripled output (266 nm) as pump pulses. The beam had a diameter of 160 µm on the sample position and the pump pulse energy at the sample was adjusted to ~ 1 µJ. Absorption changes were probed by a single-filament white light continuum generated in CaF_2 with a diameter of 100 µm on the sample. The relative orientation of pump and probe polarization time was set at the magic angle. The instrumental response time was ~180 fs (FWHM). Each scan consisted of 139 steps, from –1 to 1 ps being equidistant on a linear time scale and between 1 ps and 3.4 ns on a logarithmic time scale. 2000 spectra were recorded and a total of 4 scans were averaged for the measurement. Using a flow cell (Hellma, Suprasil) with 1 mm optical path length, sample solutions were circulated over the course of a measurement. The absorption of samples was set to ~ 0.7 per mm at the excitation wavelength. The solvent signal was recorded as a separate measurement and subtracted with proper scaling [24]. The instrumental time zero shift was determined as a function of wavelength via the optical Kerr effect and corrected for.

2.6 Nanosecond transient absorption spectroscopy

A detailed description of the setup is given elsewhere [18]. Nanosecond transient absorption spectra were acquired using an Edinburgh Instruments LP980 spectrometer in a right-angle geometry. The fourth harmonic (266 nm) pulses from a Nd:YAG laser (Spitlight 600, Innolas, 5 Hz repetition rate, pulse duration of 12 ns (FWHM)) served as the excitation. The beam had a diameter of ~8 mm. The average pulse energy was set to 2 mJ. As a probe beam a pulsed xenon lamp (Osram XBO 150 W/CR OFR) was utilized. A photomultiplier (Hamamatsu, PMT-900) was used to detect the transmitted probe light after being dispersed by a grating monochromator. Every 5 nm, kinetic traces were acquired and averaged over 64 acquisitions to obtain transient spectra. The sample solution was circulated by a peristaltic pump (REGLO Analog MS-2/8 from ISMATEC®) through a rectangular flow cell. In the direction of the pump its length amounted to 5 mm, in the probe direction to 10 mm. The samples absorption at the excitation wavelength amount to 1.6 per cm.

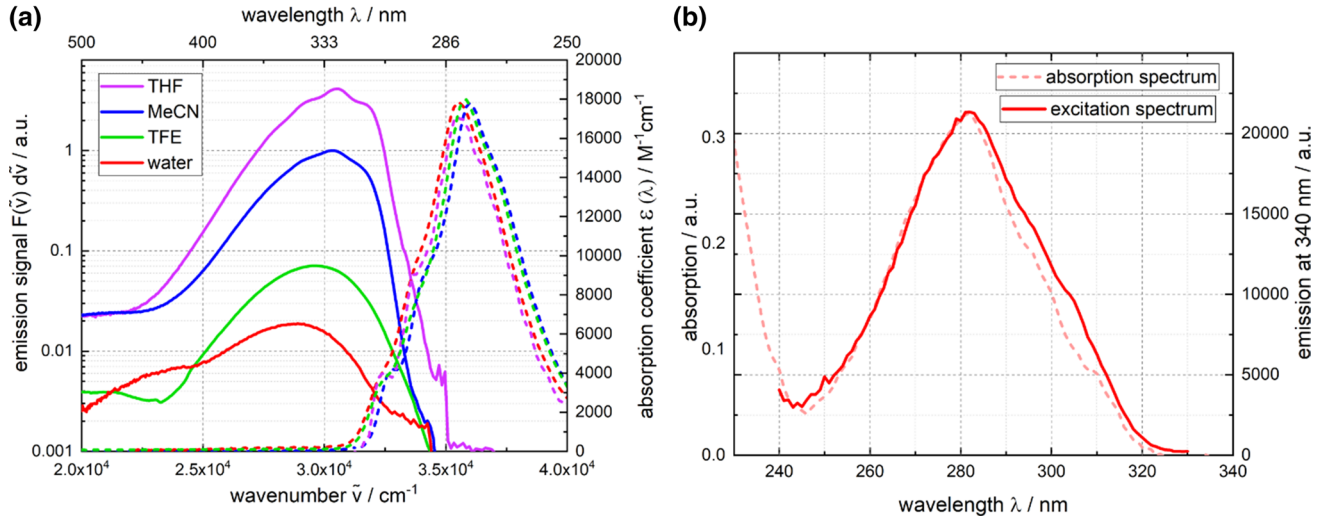

Fig. 1 **a** Fluorescence (logarithmic y-axis, solid lines) and absorption (coefficients, dashed lines) spectra of 2-CI in different solvents. The excitation wavelength for the fluorescence spectra was tuned to 260 nm. Fluorescence spectra are scaled so that their integrals are proportional to their fluorescence quantum yields Φ_{fl}. **b** Fluorescence excitation of 2-CI in comparison with its absorption spectrum. For the excitation spectrum the signal was probed at 340 nm

2.7 Data analysis

The measured data sets $S(\lambda, t)$ were analyzed globally with multi-exponential fit function convoluted with the instrumental response function (IRF):

$$S(\lambda, t) = IRF \otimes \sum_{i=1}^{n} S_i(\lambda) \cdot e^{-\frac{t}{\tau_i}}. \quad (2)$$

The procedure yields time constants τ_i, decay associated spectra $S_i(\lambda)$ (DAS, in the case of fluorescence measurements) and decay associated difference spectra (DADS, in the case of absorption measurements) [25, 26]. A spectrum $S_i(\lambda)$ parametrizes the spectral changes in the course of a process with time constant τ_i. For $S_i(\lambda) > 0$, it describes a signal decay and for $S_i(\lambda) < 0$ a rise. The sum of the spectra $S_i(\lambda)$, $\sum_{i=1}^{n} S_i(\lambda)$, equals the signal at time zero.

3 Results

3.1 Steady state spectroscopy of 2-CI in different solvents

The absorption band of 2-CI lowest in energy is located at wavenumbers larger than 30,000 cm^{-1} (see Fig. 1, Table 1 and ref. [9]). The band consists of a shoulder around 32,500 cm^{-1} and a maximum at 35,500 cm^{-1}. The absorption band features a weak positive solvatochromism, i.e., it shifts to smaller wavenumbers with increasing solvent polarity. Peak absorption coefficients ε_{max} determined here are in the range 17,000–18,000 M^{-1} cm^{-1} and depend only slightly on the solvent (see also Table 1). The present value for water of 17,800 M^{-1} cm^{-1} is somewhat higher than the value of 16,000 M^{-1} cm^{-1} reported earlier [9].

Table 1 Photophysical properties of 2-CI derived from steady-state experiments

	Water	TFE	MeCN	THF
λ_{abs}/nm	282	279	280	282
ε_{max}/ M^{-1} cm^{-1}	17,800 ± 120	17,050	17,800 ± 700	17,200 ± 570
λ_{em}/nm	342	333	329	328
Φ_{fl}	4.4×10^{-4}	1.3×10^{-3}	1.5×10^{-2}	5.7×10^{-2}
k_{rad}/s^{-1}	0.61×10^{8}	0.40×10^{8}	0.17×10^{8}	0.23×10^{8}
τ_{fl}^{SB}/ps	7	32	850	2500

Absorption maxima λ_{abs} of the absorption band lowest in energy are listed. Absorption coefficients ε_{max} correspond to the strongest absorption maxima. Wavelengths λ_{abs} and λ_{em} are retrieved from spectra obtained with constant wavelength bandpass. Experimental fluorescence quantum yields Φ_{fl} were determined with thymidine in water as a reference ($\Phi_{fl} = 1.32 \times 10^{-4}$ [16]). The radiative rate constants k_{rad} were determined via a Strickler–Berg analysis as described in the text. The last row gives predicted fluorescence lifetimes τ_{fl}^{SB}, whereby $\tau_{fl}^{SB} = \frac{\Phi_{fl}}{K_{RAD}}$

The fluorescence emission spectra of 2-CI in the different solvents peak around 30,000 cm^{-1} (see Fig. 1 and Table 1). As the absorption spectra they are subject to a weak positive solvatochromism. The impact of the solvent on the fluorescence quantum yield Φ_{fl} is pronounced. In water, it amounts to 4.4×10^{-4}. In THF, it is two orders of magnitude higher. This dependence is in agreement with previous studies

[9]. The fluorescence excitation spectra overlay favorably with the properly rescaled absorption spectrum exemplified in Fig. 1b for 2-CI in water. 2-CI, thus, obeys the Kasha-Vavilov rule [27].

To arrive at a first estimate for the excited state lifetime, particularly for 2-CI in water, a Strickler–Berg analysis was undertaken [28, 29]. For 2-CI, such an analysis is hampered by overlapping electronic transitions around 30,000 cm^{-1}. According to quantum chemical calculations [15] and gas phase spectroscopy [10] two $\pi\pi^*$ transitions termed L_a and L_b are located in this energetic region. For 2-CI, the L_b transition was found to be lowest in energy. The L_b transition features a smaller oscillator strength ($f = 0.092$) than the L_a one ($f = 0.307$) [15]. To isolate the L_b contribution to the band around 30,000 cm^{-1}, a procedure developed earlier [30] was used. The procedure rests on the assumption that a mirror image relation [29] exists between the fluorescence spectrum and that part of the absorption spectrum from which the fluorescence originates. Thus, the 2-CI fluorescence spectrum plotted on a wavenumber axis was flipped and shifted to overlay with the onset of the absorption spectrum (see Fig. 2). Hereby, the "trivial" frequency dependences of spontaneous emission (fluorescence) and absorption [29] was taken into account. The height of the flipped and shifted spectrum was scaled so that it approximately matches the absorption coefficient spectrum of 2-CI. The spectrum generated thereby entered the Strickler–Berg analysis. The radiative rate constants k_{rad} obtained are of the order of 0.5×10^8 s^{-1} (see Table 1). With these rate constants and the fluorescence quantum yields Φ_{fl}, fluorescence lifetimes τ_{fl}^{SB} can be predicted, according to $\tau_{fl}^{SB} = \frac{\Phi_{fl}}{k_{rad}}$. The lifetimes obtained for 2-CI in THF ($\tau_{fl}^{SB} = 2500$ ps) and in MeCN ($\tau_{fl}^{SB} = 850$ ps) compare favorably with the ones measured directly (2900 and 900 ps [9]). The lifetimes for the other two solvents will be considered in conjunction with the time resolved measurements.

3.2 Time resolved fluorescence spectroscopy of 2-CI in water

In previous studies on the 2-CI fluorescence [9, 10], its decay in water was not reported due to the limited time resolution of the instruments. Here, the decay is traced by femtosecond fluorescence Kerr gating [17, 18]. In these experiments, solutions of 2-CI in water were excited at 266 and 310 nm. For 266 nm excitation, 2-CI should predominately be promoted to the L_a state, the 310 nm excitation should favor L_b excitation [15]. 266 nm excitation causes a fluorescence signal peaking at 341 nm (Fig. 3) which is close to the value of the steady-state spectrum (cf. Fig. 1). The signal decays to zero on the 10 ps time scale. Closer inspection reveals a slight red-shift and broadening within ~ 1 ps. To retrieve time

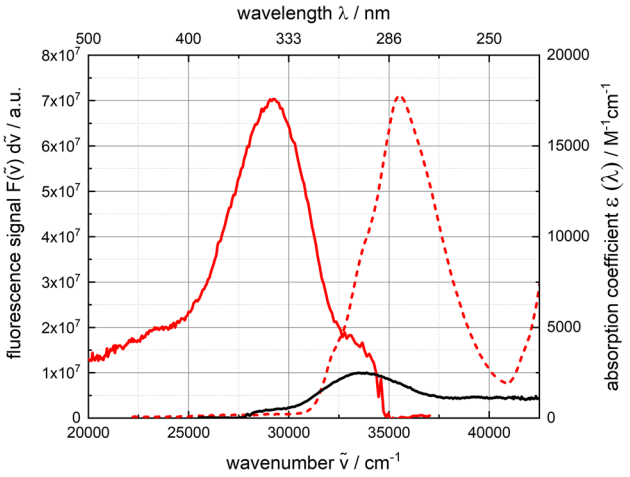

Fig. 2 Identification of the L_b band in the absorption spectrum of 2-CI in water. A synthetic absorption spectrum of the L_b state (black) was generated from the fluorescence spectrum (red) and compared with the experimental absorption spectrum (dotted red line). For details, see text

constants, the spectro-temporal behavior of the fluorescence was subject to a global analysis. A multi-exponential ansatz convoluted with instrumental response function served as a trial function. Two exponential terms proved necessary for a satisfactory fit of the measurement. The time constants retrieved are τ_{fl_1}=1.5 ps and τ_{fl_2}=7.9 ps (see Table 2). The value of τ_{fl_2} is close to the estimate based on the Strickler–Berg treatment (see above). The decay associated spectrum DAS_1 for the time constant τ_{fl_1} peaks at 328 nm and its height amounts to only ~ 1/3 of the one of DAS_2 which peaks at 351 nm (Fig. 5). By adjusting the polarization of the excitation light parallel and perpendicular positions, the time dependent anisotropy $r(t)$ was recorded. The anisotropy is close to zero throughout the time range covered.

Excitation of 2-CI in water with 310 nm pulses results in a time dependent fluorescence signal similar to the one for 266 nm excitation (Fig. 4). The emission again peaks around 341 nm and decays on the 10 ps time scale. The time constants retrieved by the global analysis amount to τ_{fl_1}= 2.5 ps and τ_{fl_2}= 7.6 ps and are, thus, close to the values for the 266 nm excitation. Also, the DAS exhibit similar shapes and relative heights (cf. Fig. 5). The time dependent anisotropy $r(t)$ does differ from the 266 nm experiment. Its initial value is 0.2. Within ~ 5 ps it decays to zero. However, after a few picoseconds the $r(t)$ curve fluctuates strongly since the fluorescence signals contributing go to zero as well. Therefore, this decay behavior of the anisotropy should not be interpreted.

Measurements with both excitation wavelengths revealed a bi-exponential decay when analyzing them with multi-exponential trial function. It is well known that on the picosecond time scale fluorescence spectra red-shift due to dielectric relaxation (dynamic Stokes shift) [31]. Such a shift

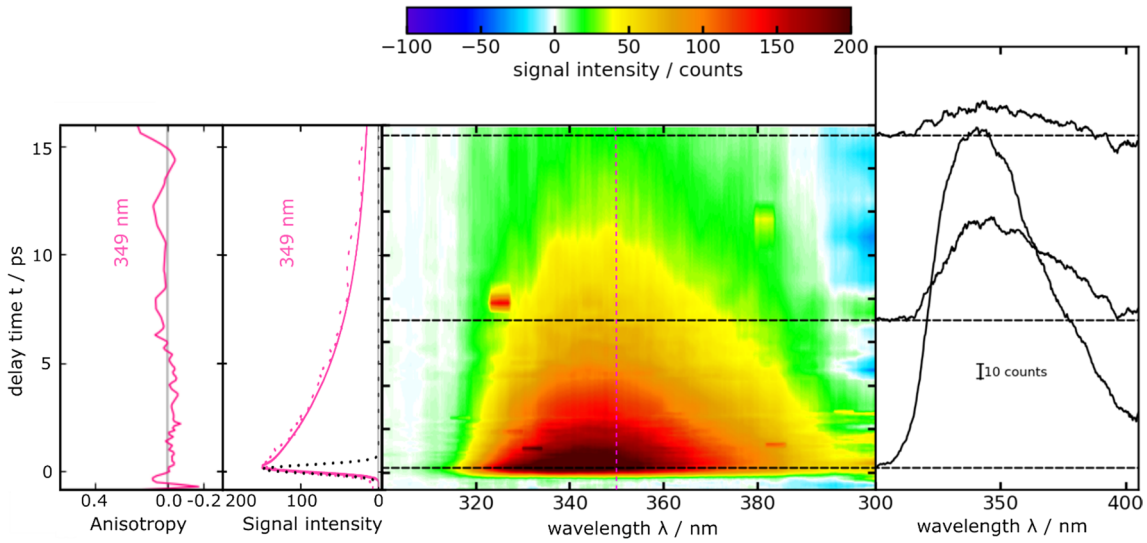

Fig. 3 Femtosecond transient fluorescence on 2-CI in water (~24 µM) as a function of detection wavelength λ and delay time t. The solution was excited at 266 nm. In the central contour representation, reddish hue represents large fluorescence signals. One representative time trace (349 nm) as well as a fit are shown on the left. The dotted black line represents the IRF as obtained from Raman scattering of the solvent. Selected spectra are depicted on the right. Their vertical positions correspond to the respective delay time. On the very left, the anisotropy as a function of time is plotted. The selected detection wavelength was 349 nm. The signal does not show a significant wavelength dependence

can "feign" a multi-exponential decay if the data set is analyzed with the trial function used here [32]. Thus, to clarify whether the bi-exponential decay is genuine, a second ansatz for the analysis was used. A normalized spectrally integrated fluorescence signal $I_{fl}(t)$ was computed according to

$$I_{fl}(t) = \frac{\int \frac{S_{fl}(\tilde{\nu},t)}{\tilde{\nu}^3} d\tilde{\nu}}{\int \frac{S_{fl}(\tilde{\nu},0)}{\tilde{\nu}^3} d\tilde{\nu}}. \quad (3)$$

Hereby, $S_{fl}(\tilde{\nu}, t)$ is the wavenumber $\tilde{\nu}$ and time t dependent fluorescence signal. $S_{fl}(\tilde{\nu}, 0)$ is this signal at time zero. The division by $\tilde{\nu}^3$ cancels the trivial wavenumber or frequency dependence [29]. The average time dependent emission wavenumber $\langle\tilde{\nu}\rangle(t)$ was computed via

$$\langle\tilde{\nu}\rangle(t) = \frac{\int \frac{S_{fl}(\tilde{\nu},t)}{\tilde{\nu}^3} \tilde{\nu} d\tilde{\nu}}{\int \frac{S_{fl}(\tilde{\nu},t)}{\tilde{\nu}^3} d\tilde{\nu}}. \quad (4)$$

As the above description has shown, the signals $S_{fl}(\tilde{\nu}, t)$ are very similar for excitation wavelengths of 266 and 310 nm. The 266 nm measurement offers a larger spectral coverage and a higher signal to noise ratio. The analysis was, thus, performed on the 266 nm measurement.

The time dependence of the spectrally integrated signal $I_{fl}(t)$ (Fig. 6) is very similar to wavelength resolved time traces depicted in Fig. 3. Indeed, a bi-exponential fit of $I_{fl}(t)$ taking the IRF into account yields time constants $\tau_{fl_1}^{int}$=1.5 ps (relative amplitude 0.4) and $\tau_{fl_2}^{int}$=8 ps (0.6) which are very close to those determined by the above global analysis. The average fluorescence wavenumber at time zero $\langle\tilde{\nu}\rangle(0)$ amounts to 29,300 cm^{-1}. It shifts to 27,900 cm^{-1} for "infinite" times. According to a single exponential fit, the time constant for this shift is 0.33 ps. This time constant is close to the average solvent relaxation time of water (0.4 ps [31]).

3.3 Time resolved UV/Vis absorption spectroscopy of 2-CI in different solvents

Obviously, time resolved fluorescence spectroscopy cannot reveal which states are populated in the course of the depletion of the primarily excited singlet state. Therefore, also time resolved UV/Vis absorption experiments were

Table 2 Summary of time constants for the decay of 2-CI in various solvents for the excitation with 266 nm

	Water	TFE	MeCN	THF
τ_1/ps	0.9	1.4	2.8	5.3
τ_2/ps	8.3	29	640	2600
τ_{fl_1}/ps	1.5 ± 0.4			
τ_{fl_2}/ps	7.9 ± 0.5			
τ_3/µs			1.56	1.56

τ_1, τ_2 obtained from femtosecond UV/Vis absorption measurements and τ_3 from nanosecond transient absorption experiments. τ_{fl_1} and τ_{fl_2} were retrieved from fs transient fluorescence measurements

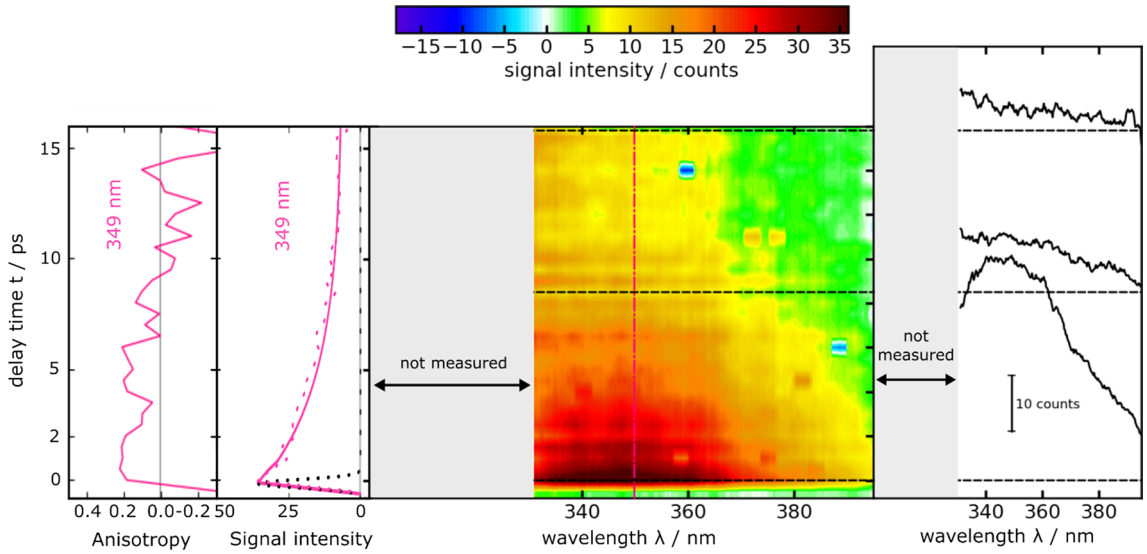

Fig. 4 Femtosecond transient fluorescence on 2-CI in water (~ 32 µM) as a function of detection wavelength and delay time. The solution was excited at 310 nm. For the description of the representation see Fig. 3

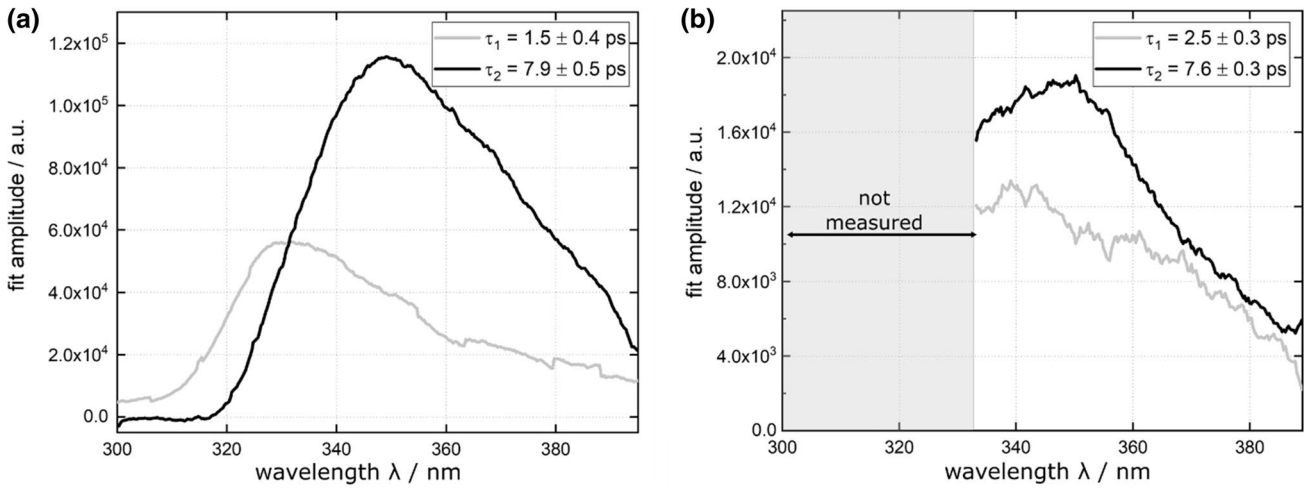

Fig. 5 Decay associated spectra derived from the fluorescence decays of 2-CI in water **a** for the excitation with 266 nm depicted in Fig. 3 and **b** for the excitation with 310 nm depicted in Fig. 4. The time constants derived from global fits are indicated

conducted. According to the above fluorescence experiments, the excitation wavelength has little impact on the decay kinetics. Therefore, for all absorption experiments, the excitation was tuned to 266 nm. For 2-CI in water, the excitation results in positive absorption changes throughout the spectral range covered (Fig. 7). No negative signals due to ground state bleach (GSB) or stimulated emission (SE) are recorded. The absence of GSB is due to small vanishing absorption coefficients of 2-CI in this range, cf. Fig. 1. The SE signal is expected in the spectral region of the fluorescence. Its absence indicates that it is overcompensated by excited state absorption (ESA). The ESA at time zero is characterized by peaks at 440 nm and ~ 750 nm. Within ~ 1 ps a slight signal decrease around 435 nm and a weak increase around 570 nm is observed. This results in a less structured difference spectrum. The overall signal decays to essentially zero on the 10 ps time scale.

The behavior in another protic solvent, namely TFE, is similar (Fig. 7). Around time zero the ESA peaks mentioned before at ~ 430 and 720 nm are observed. In addition, a positive difference absorption feature increasing toward the UV is discernible. Again, minor signal changes within a few picoseconds are recorded. The overall signal decay is slower than in water occurring with 20–30 ps. After that decay a weak absorption band peaking at 405 nm persists until the end of time range covered (3 ns).

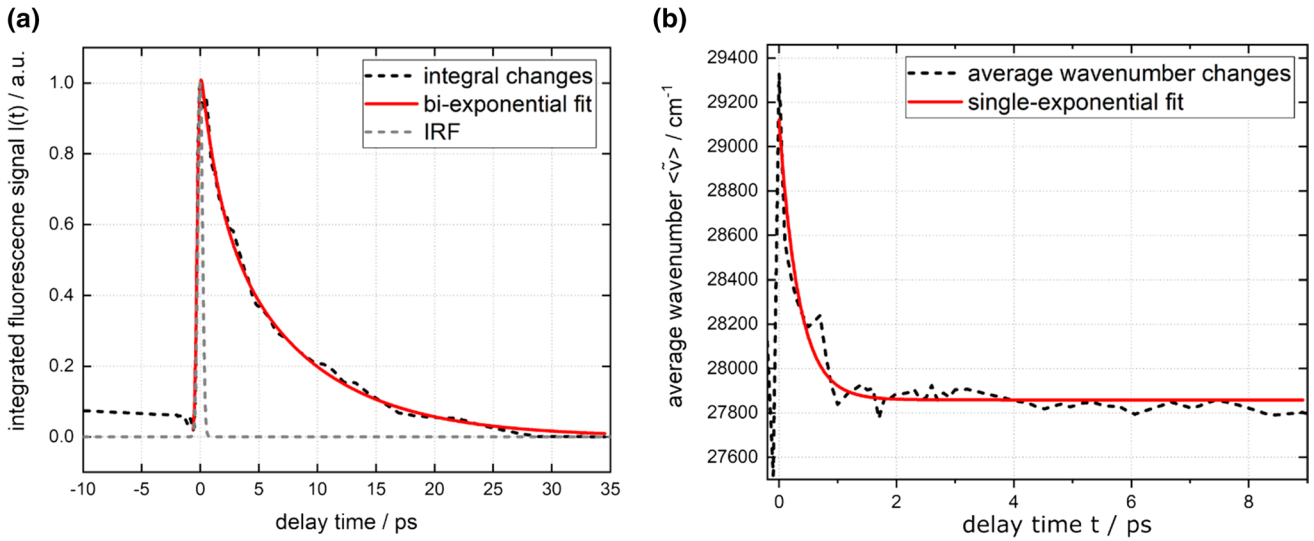

Fig. 6 Analysis of the fluorescence signal depicted in Fig. 3 using spectral integrals. **a** The spectrally integrated fluorescence signal $I_{fl}(t)$ (cf. Equation (3)) is plotted as a function of time (dotted black line). The red line represents the result of bi-exponential fit which takes the IRF into account. **b** The evolution of the average emission wavenumber $\langle\tilde{\nu}\rangle(t)$ (cf. Equation (4), dotted black line) and the result of a single-exponential fit (solid red line)

In the aprotic solvents MeCN and THF, similar spectral signatures as in the protic ones are observed around time zero (Fig. 8). Again, small spectral changes occur within a few picoseconds. The decay of the initial signature now takes much longer and occurs on the nanosecond time range. This is in line with the solvent dependence of the fluorescence lifetime reported earlier [9]. Importantly, on this time scale also a signal increase around 410 nm is observed. This rise is due to the population of a longer lived transient species—presumably the triplet state of 2-CI. According to the transient spectra at 3 ns, the species features an absorption peak at 420 nm and a shoulder at 380 nm. The same signature was observed in a nanosecond transient absorption experiment (Fig. 8). According to these experiments, the species exhibits a lifetime in the microsecond range in deoxygenated solutions (1.56 µs for 2-CI in MeCN as well as THF) which is in line with the tentative triplet assignment [33].

For a quantitative comparison of the 2-CI transient absorption in different solvents, the same analysis approach as for time resolved fluorescence was adopted. Measurements in all solvents could be fitted with a tri-exponential trial function. Hereby, one time constant was set to infinity to account for the signal persisting longer than 3 ns ("offset" in the following). The first time constant τ_1 ranges between 0.9 ps (water) and 5.3 ps (THF), see Table 2. The value for water is close to one determined by time resolved fluorescence spectroscopy (τ_{fl_1}=1.5 ps). The respective decay associated difference spectra $DADS_1$ are similar to each other with maxima around 460 nm and minima at 560 nm (Fig. 9). The minima are more pronounced in protic solvent. Relative to the other DADS the amplitudes are smaller and, thus, $DADS_1$ parametrizes small spectral changes. The second time constant τ_2 spreads between 8.3 ps (water) to 2600 ps (THF). The value for water is again very close to fluorescence time constant τ_{fl_2}=7.9 ps. The values for MeCN (τ_2 =640 ps) and THF (τ_2=2600 ps) are close to the reported fluorescence lifetimes (900 and 2900 ps [9]). In the $DADS_2$ maxima are located at 420, 560, and ~ 720 nm for the protic solvents. In the aprotic solvents, minima are found at 410 nm. These negative features parametrize the rise due to the population of a species with "infinite" lifetime. Accordingly, in the $DADS_3$ positive bands around 410 nm are seen for the aprotic solvents. For the protic ones, a weak if any signature is seen here.

4 Discussion

The essential experimental findings of this study are the first report of the fluorescence decay of 2-CI in water, the anisotropy of this fluorescence, the bi-exponential decay of the singlet state in all solvents considered as well as the population of the triplet state in aprotic solvents. Steady state (Strickler–Berg analysis) as well as time resolved fluorescence and absorption spectroscopy reveal a fluorescence lifetime of ~ 8 ps for 2-CI in water. In the Strickler–Berg analysis, one only arrives at this value when isolating the L_b contribution to the absorption band lowest in energy (cf. Fig. 2). This gives strong evidence that the emission originates from the L_b state. As all lifetimes derived via Strickler–Berg match the ones measured directly (cf. Tables 1 and 2), emission

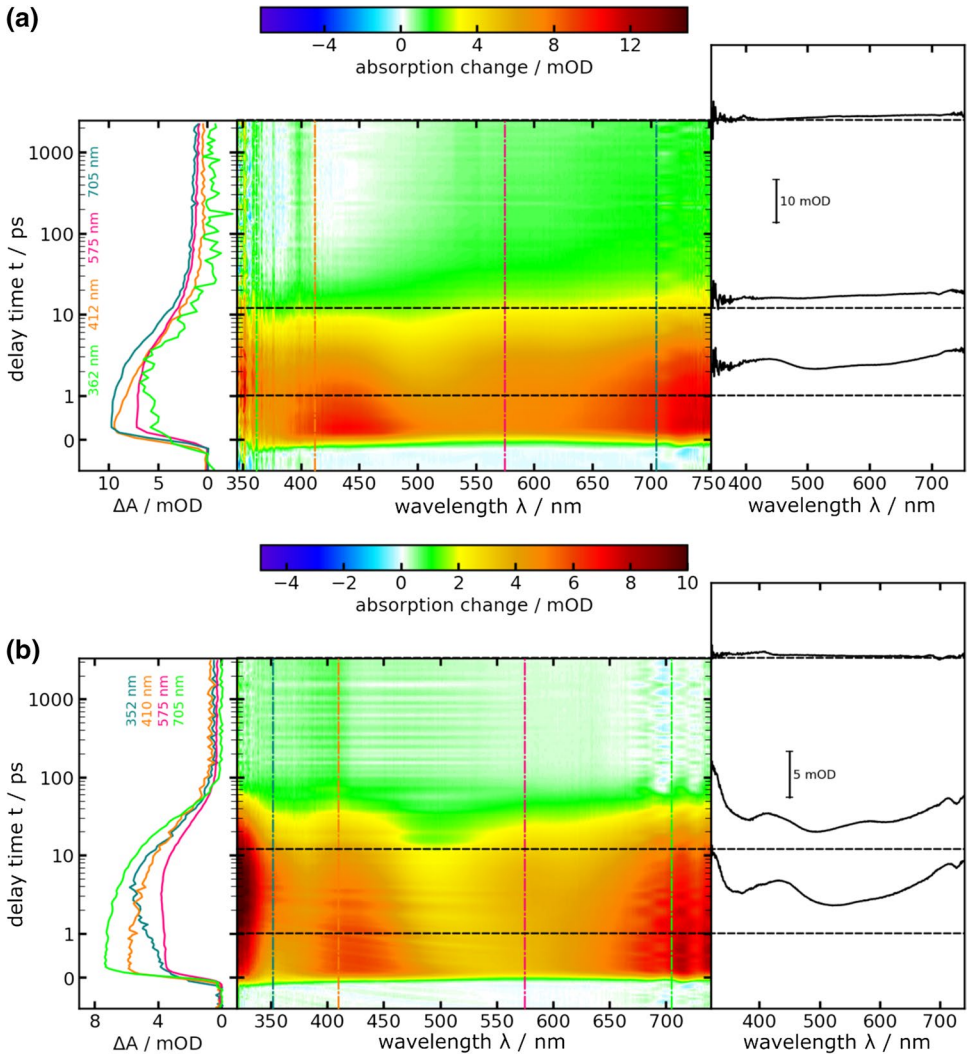

Fig. 7 Femtosecond UV/Vis absorption as a function of detection wavelength λ and delay time t on 2-CI in protic solvents. The solutions were excited at 266 nm. In the central contour representation, reddish hue stands for positive difference absorption due to ESA. The time axis is linear until 1 ps and logarithmic thereafter. Representative time traces are plotted on the left (vertical dashed lines in the contour plot indicate their spectral position). Selected difference spectra are depicted on the right. Their vertical positions (horizontal dashed lines) correspond to the respective delay time. **a** Solvent water, 2-CI concentration of 10 µM. **b** Solvent TFE, 2-CI concentration of 6.7 µM. For the measurement of 2-CI in water, the scattering of the second order excitation light from 532 to 553 nm was removed and spectra were interpolated in between

seems to occur from the L_b state in all solvents. The L_b lifetime decreases with increasing solvent polarity and proticity. The impact of the latter is particularly pronounced as a comparison of the behavior in MeCN (aprotic) and TFE (protic) shows. In MeCN (dielectric constant of 35.9 [33]) the lifetime is around 900 ps. In TFE with its smaller dielectric constant (26.7 [33]) the lifetime is around 30 ps.

The fluorescence anisotropy experiment confirms the emission out of the L_b state. With 266 nm excitation the (initial) anisotropy of the transient fluorescence is close to zero. As rotational depolarization occurs on a much longer time scale [34, 35] than the IRF time (~430 fs) of the experiment, this anisotropy value has to be related to non-parallel transition dipoles for excitation and emission. An initial anisotropy of zero implies that the two transition dipoles span an angle of 54.7° [34]. According to quantum chemical computations, the angle between the transition dipoles of the L_a and L_b states are very close to this value, namely 57° [15]. According to these computations, the 266 nm excitation addresses the L_a state. Within our IRF time (~430 fs), an internal conversion (IC) transition to the L_b state seems to occur from which all fluorescence detected here originates. Such a short transition time is in agreement with recent measurement on tryptophan, for which the $L_a \rightarrow L_b$ transition was shown to occur within less than 50 fs [36]. A similar transition time was derived from fluorescence anisotropy measurements on 5-methoxyindole [37]. The anisotropy of zero implies that also in terms of adiabatic energies the L_b state is the lowest. Thus, no L_a-L_b state switching occurs (situation as described by Fig. 8a in ref. [15]). Hebestreit et al. [10] have calculated the excited state dipole moments of the L_a and L_b state, respectively, and compared them to the experimental values from electronic Stark spectroscopy. They found a considerably smaller dipole moment for the L_a (3.44D) compared to the L_b state (4.95D) in 2-CI. This behavior is strikingly different from that of the other substituted indoles and also from the parent indole, in which the dipole moment of the L_a state is always larger than of the L_b

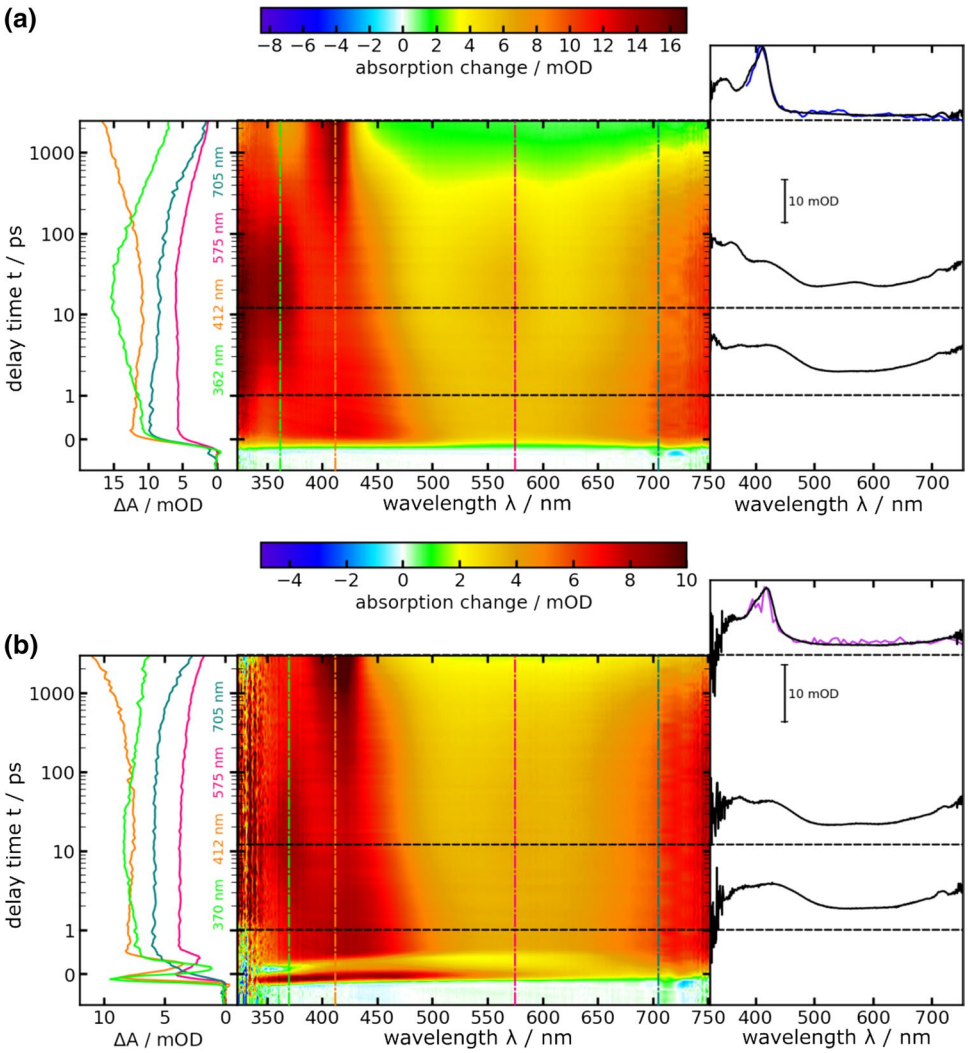

Fig. 8 Femtosecond UV/Vis absorption as a function of detection wavelength λ and delay time t on 2-CI in aprotic solvents. The solution was excited at 266 nm. For the description of the representation see Fig. 7. **a** Solvent MeCN, 2-CI concentration of 7.2 µM. **b** Solvent THF, 2-CI concentration of 11 µM. Overlaid with the spectra at 3 ns are the spectra from nanosecond transient absorption experiments (blue and purple). Neat THF exhibits strong signals around time zero which cannot be completely removed by subtraction. This explains the time zero pattern

state. Even for the structurally very similar 3- [38], 4- [39], and 5-CI [40] the L_a dipole moment is the larger one, leading to state inversion upon solvation in strongly polar solvents. It can thus be stated safely that it is the small dipole moment of the L_a state in 2-CI, which impedes state switching here. One has, however, to keep in mind that the notation of L_a and L_b for the excited ππ* states is somehow misleading, since the states tend to mix considerably and the original notation, introduced by Platt for cata-condensed hydrocarbons [41] and later extended to indole by Weber [42] is difficult to employ, the closer both ππ* states are located.

For 310 nm excitation, the (initial) anisotropy amounts to ~ 0.2. For this excitation wavelength, the L_b state is predominately excited [15] and from this state emission ought to occur. Thus, only one transition dipole is involved and the initial anisotropy should amount to 0.4 [34]. The observation that the experimental value is smaller than this prediction could be due to two reasons. (i) Even in chromophores with no overlapping electronic transitions the initial anisotropies are commonly somewhat smaller than 0.4 [1]. This matches our observation on the anisotropy behavior of thymidine in water which was investigated for calibration purposes (see Experimental Section). For thymidine, an initial anisotropy of 0.4 is expected. Our measurement yielded a value of ~ 0.3 in good agreement with an earlier study [20]. (ii) The L_a and L_b transition partially overlap and the L_a transition exhibit a much larger oscillator strength. Therefore, it is very likely that with the 310 nm excitation the L_b state is not excited exclusively. As discussed above a partial L_a excitation ought to shift the anisotropy toward zero. Presumably both contributions are responsible for the value of 0.2 for the 310 nm excitation.

These anisotropy experiments give clear evidence that for 2-CI in water the L_b state is populated within less than ~ 100 fs irrespective of the excitation wavelength. The similarity of the transient absorption signatures around time zero and the above Strickler–Berg argument strongly suggest that this also implies for all other solvents. The depopulation of the L_b state (time constant τ_2) occurs within ~ 8 ps to ~ 2500 ps, depending on the solvent. This depopulation

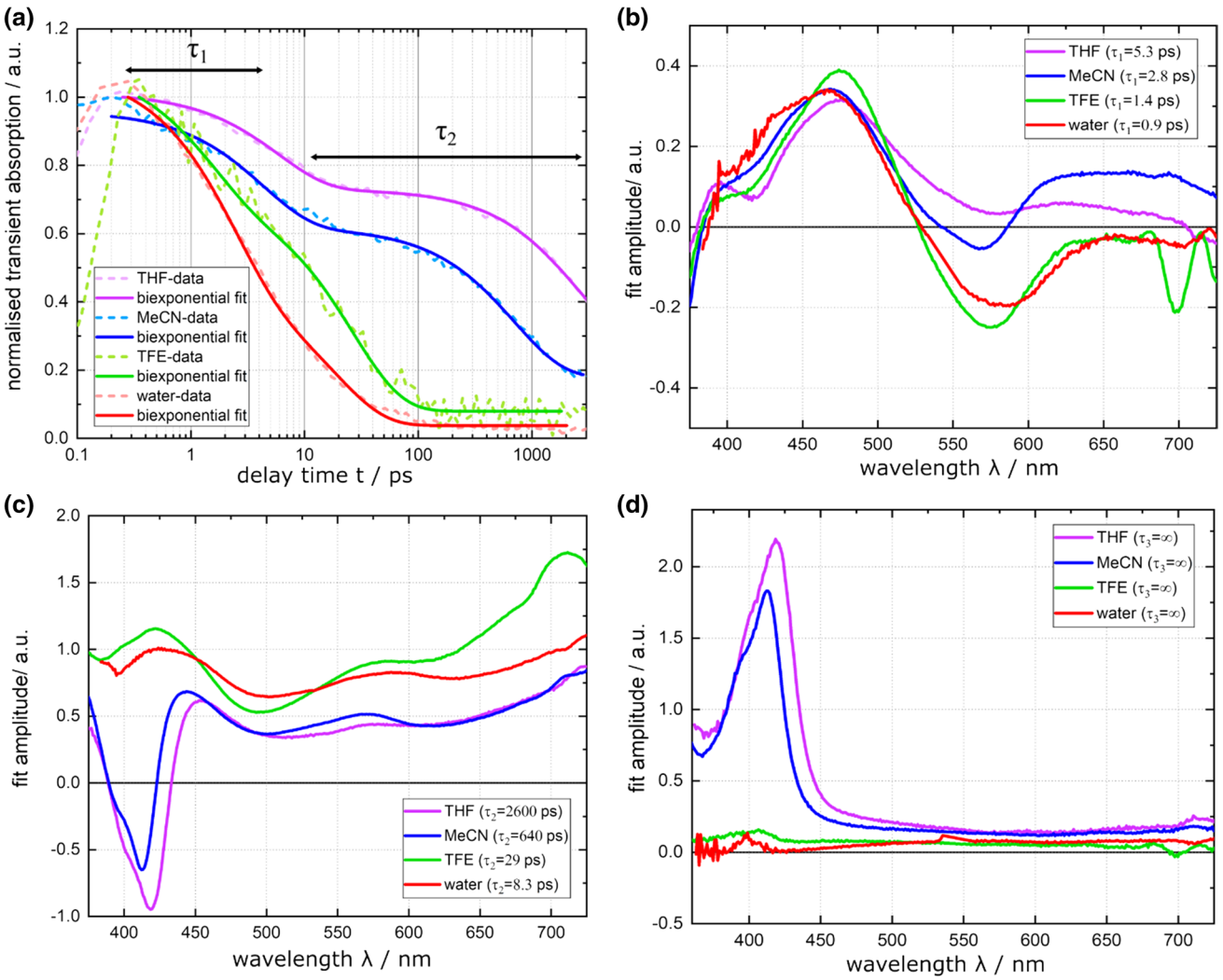

Fig. 9 Global analysis of the femtosecond UV/Vis absorption measurements on 2-CI in the four solvents as depicted in Figs. 7 and 8. **a** Time traces for a detection wavelength of 450 nm. The dashed lines are experimental values, the lines describe the fit results. The black arrows mark the spread of the time constants τ_1 and τ_2. **b** Decay associated difference spectra for the time constant τ_1, $DADS_1$. **c** $DADS_2$. **d** $DADS_3$, offset

goes along with the fluorescence decay. The solvent dependence of the time constant τ_2 can be rationalized by a crossing of the L_b state with a $^1\pi\sigma^*$ one as put forth by Domcke and Sobolewski [43, 44]. The $^1\pi\sigma^*$ state gets stabilized in polar solvents, thereby reducing the barrier for the IC transition. The present results indicate that in addition to the polarity also the proticity of the solvents has a huge impact on the lifetime τ_2. Gas phase data have shown that 2-CI forms binary cluster with water. Water seems to act as a hydrogen bond acceptor in this cluster [45]. For the isolated 3-CI-$(H_2O)_1$ cluster a direct lifetime measurement shows a distinct shortening of the fluorescence lifetime from 9.8 ns (monomer) to 3.6 ns (1:1 water cluster) [38]. Determination of fluorescence lifetimes for different cluster sizes and different solvent clusters are on the way to resolve the problem of how the solvent influences the fate of the excited state.

Prior to that a process with the time constant τ_1 of a few picoseconds occurs in all solvents. The analysis based on band integrals (cf. Fig. 6) excludes a dynamic Stokes shift as the underlying mechanism. Also, for the other solvents, the dynamic Stokes shift is an unlikely explanation. In acetonitrile, for instance, the time constant τ_1 amounts to 2.8 ps as compared to 0.9 ps for water, despite the fact that dielectric relaxation in acetonitrile is even faster than in water [31]. The underlying process might be vibrational cooling which is known to occur on the picosecond time scale [46, 47]. Yet, also vibrational cooling ought to retain the band integral [47–49]. Furthermore, for 2-CI in water, the τ_1 process is

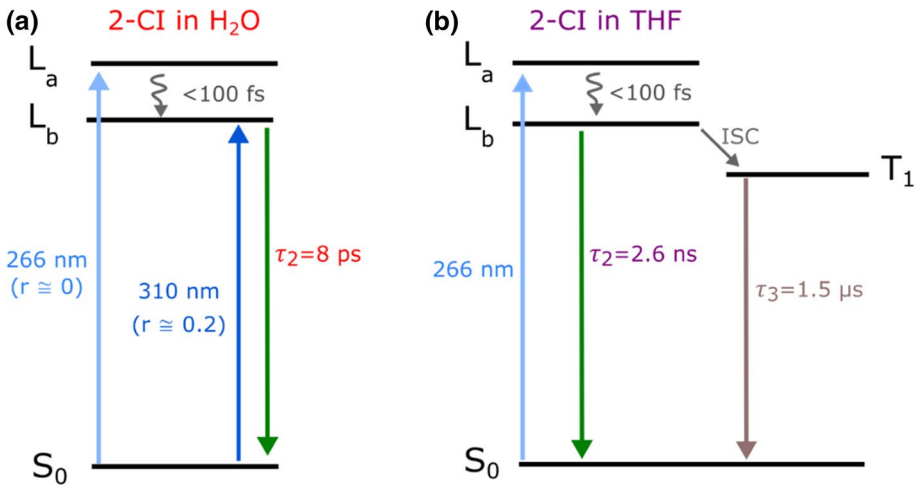

Fig. 10 Jablonski diagram of the excited state deactivation kinetics of 2-CI **a** in water and **b** THF

observed for 266 and 310 nm excitation. The 266 nm excitation deposits ~ 5000 cm^{-1} more vibrational excess energy in the molecule than the 310 nm one. If the τ_1 process were related to vibrational cooling, it should be less pronounced for 310 nm excitation. As this is not the case (cf. Fig. 5), vibrational cooling as the underlying process seems unlikely. Considering the rigid structure of 2-CI, different conformers and thereby a kinetic heterogeneity do not seem to be a plausible explanation. Aggregation can also cause such a heterogeneity [50, 51]. Yet, aggregation is expected to be solvent dependent [52–55]. As a bi-exponential behavior with similar relative amplitudes is observed in all solvents considered, also aggregation is not a probable explanation. Thus, at present, no consistent assignment can be given.

The assignment of the time constant τ_3 is less involved. The respective transient peaks around 420 nm (cf. Fig. 8) which are close to the absorption peak of the indole triplet in water [56–60]. In the respective experiments on indole [57], the triplet signature was accompanied by the ones of the indole cation and the solvated electron. In the femto- and nanosecond experiments on 2-CI these signatures are absent. This might be related with the strong electron withdrawing character of the cyano substituent. The measured time constant τ_3 for 2-CI in MeCN and THF is well in line with triplet lifetimes in general [33]. For indole and derivatives lifetimes in the range 12–50 µs were reported [56–58, 60, 61]. The value of ~ 2 µs is, thus, on the shorter side. We assign the species decaying with the time constant τ_3 to the triplet state of 2-CI. The signal of this state is nearly negligible in water as well as TFE and much larger in MeCN and THF (see $DADS_3$ in Fig. 9). As at present, no difference absorption coefficients of the 2-CI triplet are available, the triplet quantum yield Φ_T cannot be quantified. Assuming that the difference absorption coefficients are similar in all solvents and normalizing to identical excitation conditions, one can derive the following relative yields (with respect to MeCN): water (0.008), TFE (0.034), MeCN (1), and THF (0.7). Thus, triplet yields scale approximately as the lifetimes τ_2. This suggests that the rate constant (k_{ISC}) for intersystem crossing is similar in all solvents. In protic solvents, ISC is outcompeted by IC.

5 Conclusion

Femtosecond transient fluorescence experiments on 2-CI in water revealed a fluorescence decay of ~8 ps for both excitation wavelengths of 266 and 310 nm (see Fig. 10). This is a result of the ultrafast depletion of the L_a state in less than 100 fs. The respective anisotropy experiments provided strong evidence of the origin of this emission from the L_b state, regardless of the excitation wavelength. In time resolved transient absorption measurements, for all solvents, a bi-exponential decay was observed. The longer of the two (τ_2) proved to be strongly solvent dependent. In aprotic solvents (MeCN and THF), intersystem crossing to the triplet state contributes to the singlet decay. The triplet assignment was confirmed by nanosecond transient absorption experiments. The relative triplet yields are proportional to the lifetime τ_2. Quantum chemical computations aiming at the nature of the τ_1 process including channels through the $^1\pi\sigma^*$ state are under way.

Acknowledgements This work has been supported by the Deutsche Forschungsgemeinschaft (DFG, German Research Foundation), project numbers 396890929 (GRK 2482, "ModISC") and SCHM1043/14-1.

Funding Open Access funding enabled and organized by Projekt DEAL.

Data availability The datasets generated during and/or analysed during the current study are available from the corresponding author on reasonable request.

Declarations

Conflict of interest On behalf of all authors, the corresponding author states that there is no conflict of interest.

References

1. Lakowicz, J. R. (2006). *Principles of Fluorescence Spectroscopy* (3rd ed.). Springer.
2. Beechem, J. M., & Brand, L. (1985). Time-resolved fluorescence of proteins. *Annual review of biochemistry, 54*(1), 43–71. https://doi.org/10.1146/annurev.bi.54.070185.000355
3. Chen, Y., Liu, B., Yu, H.-T., & Barkley, M. D. (1996). The peptide bond quenches indole fluorescence. *Journal of the American Chemical Society, 118*(39), 9271–9278. https://doi.org/10.1021/ja961307u
4. Hu, J. J., He, P. Y., & Li, Y. M. (2021). Chemical modifications of tryptophan residues in peptides and proteins. *Journal of Peptide Science, 27*(1), e3286. https://doi.org/10.1002/psc.3286
5. Ladokhin, A. S. (2000). Fluorescence spectroscopy in peptide and protein analysis. *Encyclopedia of analytical chemistry* (pp. 5762–5779). John Wiley & Sons.
6. Xiong, Y., Shi, C., Li, L., Tang, Y., Zhang, X., Liao, S., Zhang, B., Sun, C., & Ren, C. (2021). A review on recent advances in amino acid and peptide-based fluorescence and its potential applications. *New Journal of Chemistry, 45*, 15180–15194. https://doi.org/10.1039/D1NJ02230J
7. Hansch, C., Leo, A., & Taft, R. W. (1991). A survey of Hammett substituent constants and resonance and field parameters. *Chemical Reviews, 91*(2), 165–195. https://doi.org/10.1021/cr00002a004
8. Talukder, P., Chen, S., Roy, B., Yakovchuk, P., Spiering, M. M., Alam, M. P., Madathil, M. M., Bhattacharya, C., Benkovic, S. J., & Hecht, S. M. (2015). Cyanotryptophans as novel fluorescent probes for studying protein conformational changes and DNA–Protein interaction. *Biochemistry, 54*(51), 7457–7469. https://doi.org/10.1021/acs.biochem.5b01085
9. Hilaire, M. R., Mukherjee, D., Troxler, T., & Gai, F. (2017). Solvent dependence of cyanoindole fluorescence lifetime. *Chemical Physics Letters, 685*, 133–138. https://doi.org/10.1016/j.cplett.2017.07.038
10. Hebestreit, M. L., Lartian, H., Henrichs, C., Kühnemuth, R., Meerts, W. L., & Schmitt, M. (2021). Excited state dipole moments and lifetimes of 2-cyanoindole from rotationally resolved electronic Stark spectroscopy. *Physical Chemistry Chemical Physics, 23*(17), 10196–10204. https://doi.org/10.1039/D1CP00097G
11. Ma, J., Pazos, I. M., Zhang, W., Culik, R. M., & Gai, F. (2015). Site-specific infrared probes of proteins. *Annual Review of Physical Chemistry, 66*, 357.
12. Liu, J., Feng, R.-R., Zhou, L., Gai, F., & Zhang, W. (2022). Photoenhancement of the C≡ N stretching vibration intensity of aromatic nitriles. *The Journal of Physical Chemistry Letters, 13*, 9745–9751. https://doi.org/10.1021/acs.jpclett.2c02418
13. Van Wilderen, L., Brunst, H., Gustmann, H., Wachtveitl, J., Broos, J., & Bredenbeck, J. (2018). Cyano-tryptophans as dual infrared and fluorescence spectroscopic labels to assess structural dynamics in proteins. *Physical Chemistry Chemical Physics, 20*(30), 19906–19915. https://doi.org/10.1039/C8CP00846A
14. Ahmed, I. A., Acharyya, A., Eng, C. M., Rodgers, J. M., DeGrado, W. F., Jo, H., & Gai, F. (2019). 4-Cyanoindole-2′-deoxyribonucleoside as a dual fluorescence and infrared probe of DNA structure and dynamics. *Molecules, 24*(3), 602. https://doi.org/10.3390/molecules24030602
15. Abou-Hatab, S., & Matsika, S. (2019). Theoretical investigation of positional substitution and solvent effects on n-Cyanoindole fluorescent probes. *The Journal of Physical Chemistry B, 123*(34), 7424–7435. https://doi.org/10.1021/acs.jpcb.9b05961
16. Onidas, D., Markovitsi, D., Marguet, S., Sharonov, A., & Gustavsson, T. (2002). Fluorescence properties of DNA nucleosides and nucleotides: A refined steady-state and femtosecond investigation. *The Journal of Physical Chemistry B, 106*(43), 11367–11374. https://doi.org/10.1021/jp026063g
17. Schmidt, B., Laimgruber, S., Zinth, W., & Gilch, P. (2003). A broadband Kerr shutter for femtosecond fluorescence spectroscopy. *Applied Physics B-Lasers and Optics, 76*(8), 809. https://doi.org/10.1007/s00340-003-1230-7
18. Haselbach, W., Kaminski, J. M., Kloeters, L. N., Müller, T. J. J., Weingart, O., Marian, C. M., Gilch, P., & Nogueira de Faria, B. E. (2022). Investigating a TADF emitter by time resolved near infrared spectroscopy. *Chemistry-A European Journal*. https://doi.org/10.1002/chem.202202809.
19. Kozma, I. Z., Krok, P., & Riedle, E. (2005). Direct measurement of the group-velocity mismatch and derivation of the refractive-index dispersion for a variety of solvents in the ultraviolet. *Journal of the Optical Society of America B, 22*(7), 1479–1485. https://doi.org/10.1364/JOSAB.22.001479
20. Gustavsson, T., Sharonov, A., & Markovitsi, D. (2002). Thymine, thymidine and thymidine 5′-monophosphate studied by femtosecond fluorescence upconversion spectroscopy. *Chemical Physics Letters, 351*(3), 195–200. https://doi.org/10.1016/S0009-2614(01)01375-6
21. Laimgruber, S., Schachenmayr, H., Schmidt, B., Zinth, W., & Gilch, P. (2006). A femtosecond stimulated Raman spectrograph for the near ultraviolet. *Applied Physics B, 85*(4), 557–564. https://doi.org/10.1007/s00340-006-2386-8
22. Laimgruber, S., Schmierer, T., Gilch, P., Kiewisch, K., & Neugebauer, J. (2008). The ketene intermediate in the photochemistry of ortho-nitrobenzaldehyde. *Physical Chemistry Chemical Physics, 10*(26), 3872–3882. https://doi.org/10.1039/B800616D
23. Fröbel, S., Buschhaus, L., Villnow, T., Weingart, O., & Gilch, P. (2015). The photoformation of a phthalide: A ketene intermediate traced by FSRS. *Physical Chemistry Chemical Physics, 17*(1), 376–386. https://doi.org/10.1039/C4CP03351E
24. Lorenc, M., Ziolek, M., Naskrecki, R., Karolczak, J., Kubicki, J., & Maciejewski, A. (2002). Artifacts in femtosecond transient absorption spectroscopy. *Applied Physics B, 74*(1), 19–27. https://doi.org/10.1007/s003400100750
25. Satzger, H., & Zinth, W. (2003). Visualization of transient absorption dynamics–towards a qualitative view of complex reaction kinetics. *Chemical Physics, 295*(3), 287–295. https://doi.org/10.1016/j.chemphys.2003.08.012
26. van Stokkum, I. H., Larsen, D. S., & Van Grondelle, R. (2004). Global and target analysis of time-resolved spectra. *Biochimica et Biophysica Acta -Bioenergetics, 1657*(2–3), 82–104. https://doi.org/10.1016/j.bbabio.2004.04.011

27. Klán, P., & Wirz, J. (2009). *Photochemistry of Organic Compounds. From Concepts to Practice*. Wiley.
28. Strickler, S. J., & Berg, R. A. (1962). Relationship between absorption intensity and fluoresence lifetime of molecules. *The Journal of Chemical Physics, 37*, 814–822. https://doi.org/10.1063/1.1733166
29. Parson, W. W. (2009). *Modern Optical Spectroscopy, With Exercises and Examples from Biophysics and Biochemistry* (Student). Springer.
30. Reiffers, A., Torres Ziegenbein, C., Schubert, L., Diekmann, J., Thom, K. A., Kühnemuth, R., Griesbeck, A., Weingart, O., & Gilch, P. (2019). On the large apparent Stokes shift of phthalimides. *Physical Chemistry Chemical Physics, 21*(9), 4839–4853. https://doi.org/10.1039/C8CP07795A
31. Bagchi, B., & Jana, B. (2010). Solvation dynamics in dipolar liquids. *Chemical Society Reviews, 39*(6), 1936–1954. https://doi.org/10.1039/B902048A
32. Marciniak, H., & Lochbrunner, S. (2014). On the interpretation of decay associated spectra in the presence of time dependent spectral shifts. *Chemical Physics Letters, 609*, 184–188. https://doi.org/10.1016/j.cplett.2014.05.006
33. Montalti, M., & Murov, S. L. (2006). *Handbook of photochemistry*. Taylor & Francis.
34. Kawski, A. (1993). Fluorescence anisotropy: Theory and applications of rotational depolarization. *Critical Reviews in Analytical Chemistry, 23*(6), 459–529. https://doi.org/10.1080/10408349308051654
35. Sahoo, H. (2022). Optical spectroscopic and microscopic techniques. *Springer Singapore*. https://doi.org/10.1007/978-981-16-4550-1
36. Jaiswal, V. K., Kabaciński, P., Nogueira de Faria, B. E., Gentile, M., de Paula, A. M., Borrego-Varillas, R., Nenov, A., Conti, I., Cerullo, G., & Garavelli, M. (2022). Environment-driven coherent population transfer governs the ultrafast photophysics of tryptophan. *Journal of the American Chemical Society*. https://doi.org/10.1021/jacs.2c04565
37. Shen, X., & Knutson, J. R. (2001). Femtosecond internal conversion and reorientation of 5-methoxyindole in hexadecane. *Chemical Physics Letters, 339*(3–4), 191–196. https://doi.org/10.1016/S0009-2614(01)00325-6
38. Schneider, M., Hebestreit, M.-L., Lindic, M. M., Parsian, H., Torres-Boy, A. Y., Álvarez-Valtierra, L., Meerts, W. L., Kühnemuth, R., & Schmitt, M. (2018). Rotationally resolved electronic spectroscopy of 3-cyanoindole and the 3-cyanoindole–water complex. *Physical Chemistry Chemical Physics, 20*(36), 23441–23452. https://doi.org/10.1039/C8CP04020F
39. Hebestreit, M.-L., Schneider, M., Lartian, H., Betz, V., Heinrich, M., Lindic, M., Choi, M. Y., & Schmitt, M. (2019). Structures, dipole moments and excited state lifetime of isolated 4-cyanoindole in its ground and lowest electronically excited singlet states. *Physical Chemistry Chemical Physics, 21*(27), 14766–14774. https://doi.org/10.1039/C9CP01618J
40. Oeltermann, O., Brand, C., Engels, B., Tatchen, J., & Schmitt, M. (2012). The structure of 5-cyanoindole in the ground and the lowest electronically excited singlet states, deduced from rotationally resolved electronic spectroscopy and ab initio theory. *Physical Chemistry Chemical Physics, 14*(29), 10266–10270. https://doi.org/10.1039/C2CP41094J
41. Platt, J. R. (1949). Classification of spectra of cata-condensed hydrocarbons. *The Journal of chemical physics, 17*(5), 484–495. https://doi.org/10.1063/1.1747293
42. Weber, G. (1960). Fluorescence-polarization spectrum and electronic-energy transfer in tyrosine, tryptophan and related compounds. *Biochemical Journal, 75*(2), 335.
43. Sobolewski, A. L., & Domcke, W. (1999). Ab initio investigations on the photophysics of indole. *Chemical Physics Letters, 315*(3–4), 293–298. https://doi.org/10.1016/S0009-2614(99)01249-X
44. Soboleski, A., Domcke, W., Dedonder-Lardeux, C., & Jouvet, C. (2002). Excited-state hydrogen detachment and hydrogen transfer driven by repulsive $^1\pi\sigma^*$ states: A new paradigm for nonradiative decay in aromatic biomolecules. *Physical Chemistry Chemical Physics, 4*, 1093–1100. https://doi.org/10.1039/B110941N
45. Henrichs, C., Zimmermann, S., Hebestreit, M.-L., & Schmitt, M. (2021). Excited state structure of isolated 2-cyanoindole and the binary 2-cyanoindole-(H2O) 1 cluster from a combined Franck-Condon and rotational constants fit. *Journal of Molecular Structure, 1233*, 130055. https://doi.org/10.1016/j.molstruc.2021.130055
46. Elsaesser, T., & Kaiser, W. (1991). Vibrational and vibronic relaxation of large polyatomic-molecules in liquids. *Annual Review of Physical Chemistry, 42*, 83–107. https://doi.org/10.1146/annurev.pc.42.100191.000503
47. Kovalenko, S. A., Schanz, R., Hennig, H., & Ernsting, N. P. (2001). Cooling dynamics of an optically excited molecular probe in solution from femtosecond broadband transient absorption spectroscopy. *Journal of Chemical Physics, 115*(7), 3256–3273. https://doi.org/10.1063/1.1380696
48. Schmierer, T., Schreier, W. J., Koller, F. O., Schrader, T. E., & Gilch, P. (2009). Impact of vibrational excitation on the kinetics of a nascent ketene. *Physical Chemistry Chemical Physics, 11*(48), 11596–11607. https://doi.org/10.1039/B915451E
49. Joens, J. A. (1993). Sum rule methods for the approximation of continuous electronic absorption spectra. *The Journal of Physical Chemistry, 97*(11), 2527–2534. https://doi.org/10.1021/j100113a011
50. Barzda, V., de Grauw, C. J., Vroom, J., Kleima, F. J., van Grondelle, R., van Amerongen, H., & Gerritsen, H. C. (2001). Fluorescence lifetime heterogeneity in aggregates of LHCII revealed by time-resolved microscopy. *Biophysical Journal, 81*(1), 538–546. https://doi.org/10.1016/S0006-3495(01)75720-7
51. Yan, Z.-Q., Yang, Z.-Y., Wang, H., Li, A.-W., Wang, L.-P., Yang, H., & Gao, B.-R. (2011). Study of aggregation induced emission of cyano-substituted oligo (p-phenylenevinylene) by femtosecond time resolved fluorescence. *Spectrochimica Acta Part A: Molecular Biomolecular Spectroscopy, 78*(5), 1640–1645. https://doi.org/10.1016/j.saa.2011.01.056
52. Nath, S., Pal, H., & Sapre, A. V. (2000). Effect of solvent polarity on the aggregation of C60. *Chemical Physics Letters, 327*(3–4), 143–148. https://doi.org/10.1016/S0009-2614(00)00863-0
53. Huang, H., Liang, C. H., & Penner-Hahn, J. E. (1998). X-Ray absorption spectroscopy of dimethylcuprates: Evidence for solvent-dependent aggregation. *Angewandte Chemie International Edition, 37*(11), 1564–1566. https://doi.org/10.1002/(SICI)1521-3773(19980619)37:11%3C1564::AID-ANIE1564%3E3.0.CO;2-5
54. Wang, S., & Bazan, G. C. (2004). Solvent-dependent aggregation of a water-soluble poly (fluorene) controls energy transfer to chromophore-labeled DNA. *Chemical Communications, 21*, 2508–2509. https://doi.org/10.1039/B410002F
55. Gao, B.-R., Wang, H.-Y., Hao, Y.-W., Fu, L.-M., Fang, H.-H., Jiang, Y., Wang, L., Chen, Q.-D., Xia, H., & Pan, L.-Y. (2010). Time-resolved fluorescence study of aggregation-induced emission enhancement by restriction of intramolecular charge transfer state. *The Journal of Physical Chemistry B, 114*(1), 128–134. https://doi.org/10.1021/jp909063d
56. Fischer, C. J., Gafni, A., Steel, D. G., & Schauerte, J. A. (2002). The triplet-state lifetime of indole in aqueous and viscous environments: significance to the interpretation of room temperature phosphorescence in proteins. *Journal of the American Chemical Society, 35*, 10359–10366. https://doi.org/10.1021/ja016609x
57. Bent, D. V., & Hayon, E. (1975). Excited state chemistry of aromatic amino acids and related peptides. III. Tryptophan. *Journal*

of the American Chemical Society, 97(10), 2612–2619. https://doi.org/10.1021/ja00843a004
58. Kowalska-Baron, A., Chan, M., Gałęcki, K., & Wysocki, S. (2012). Photophysics of indole, tryptophan and N-acetyl-L-tryptophanamide (NATA): Heavy atom effect. *Spectrochimica Acta Part A: Molecular Biomolecular Spectroscopy, 98*, 282–289. https://doi.org/10.1016/j.saa.2012.08.017
59. Galley, W. C., & Purkey, R. M. (1970). Role of heterogeneity of the solvation site in electronic spectra in solution. *Proceedings of the National Academy of Sciences, 67*(3), 1116–1121. https://doi.org/10.1073/pnas.67.3.1116
60. Pernot, C., & Lindqvist, L. JJo. P. (1976). Laser photolysis of indole in cyclohexane. *Joural of Photochemistry, 6*(3), 215–220. https://doi.org/10.1016/0047-2670(76)85066-6
61. Kowalska-Baron, A., Choudhary, P., & Montes, D. (2011). The effect of immobilization in the PVA films on the fluorescence and phosphorescence lifetime of indole and its derivatives. *Biotechnology Food Science, 2*, 3–14. https://doi.org/10.34658/bfs.2011.75.2.3-14